Non-Invasive Wearable RF Device towards Monitoring Brain Atrophy and Lateral Ventricle Enlargement

Non-Invasive Wearable RF Device Towards Monitoring Brain Atrophy and Lateral Ventricle Enlargement

Imran M. Saied, Tughrul Arslan, *Senior Member, IEEE*

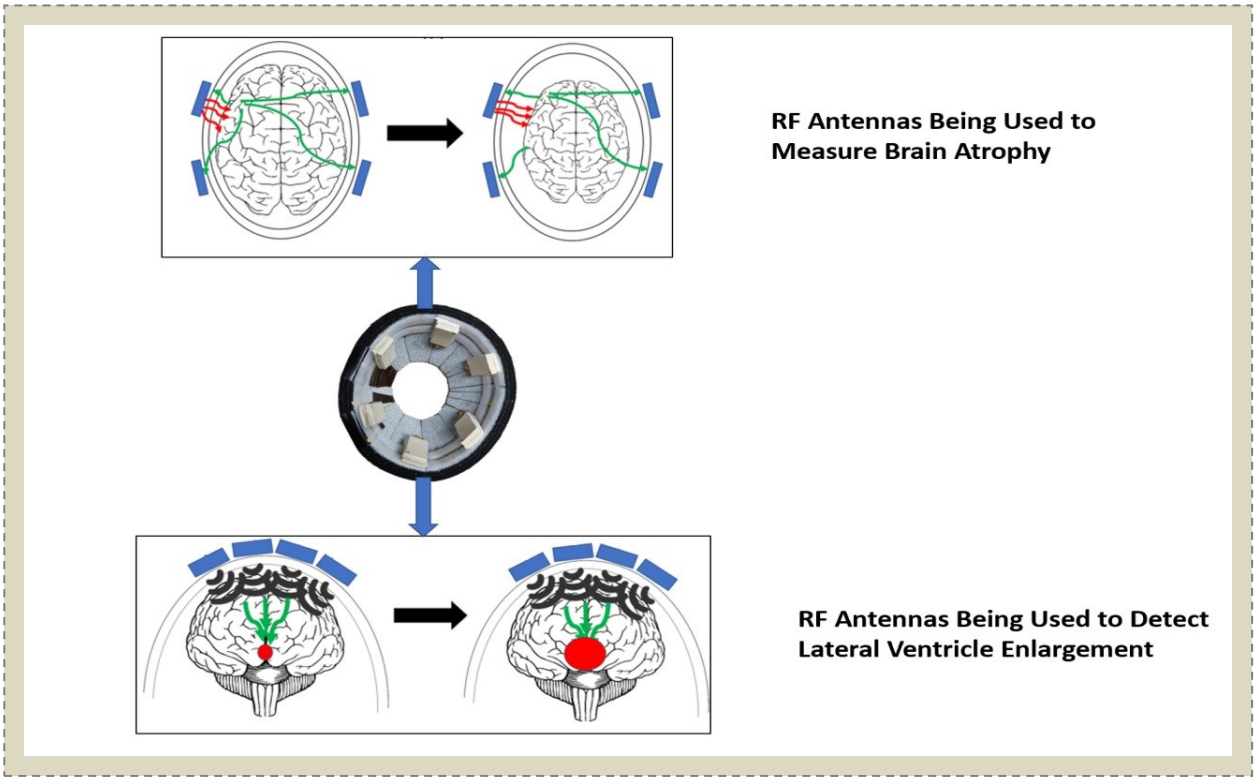

Flexible UWB monopole antennas were implemented in a wearable head device and tested for measuring and detecting brain atrophy and lateral ventricle enlargement for patients with Alzheimer's disease.

Take-Home Messages

- A wearable device was developed with electromagnetic sensors in order to non-invasively monitor the progress of brain atrophy and lateral ventricle enlargement as a result of Alzheimer's disease.
- The developed wearable RF device is capable of detecting the progression of brain atrophy and lateral ventricle enlargement successfully.
- The work in this study targets Alzheimer's disease and aims to develop a non-invasive device for monitoring the progression of the disease in patients.
- The breakthrough in this work is the development of a wearable device that uses RF sensors for detecting changes in the brain as a result of Alzheimer's disease.

Non-Invasive Wearable RF Device towards Monitoring Brain Atrophy and Lateral Ventricle Enlargement

Imran M. Saied, Tughrul Arslan, *Senior Member, IEEE*

***Abstract* -** Alzheimer's disease is the most common form of neurodegenerative disease and a leading cause of dementia today. A pathological effect of Alzheimer's disease is brain atrophy, which is the progressive shrinkage of the brain volume and weight. Another effect of Alzheimer's disease is the enlargement of lateral ventricles in the brain. Currently, MRI and CT scanners can detect and show images of the brain during different stages of Alzheimer's disease. However, its limited accessibility, high costs, and static structure make it inconvenient for some to use. This paper presents the design and novel application of a wearable device comprising of flexible microwave antennas, with an operating frequency range of 800 MHz to 2.5 GHz, that detects the progression of brain atrophy and lateral ventricle enlargement in patients with Alzheimer's at the earliest stage possible. The operating principle of the antennas are simulated in near field using CST and the device is experimentally validated using lamb brain samples and samples representing cerebral spinal fluid (CSF). The measured reflection coefficients (S_{11}) and transmission coefficients (S_{21}) were found to correlate with changes in brain volume and changes in CSF volume successfully, thus giving an indication of the progression of Alzheimer's disease in a patient.

***Keywords* — Electromagnetic, RF sensing, microwave medical imaging, RF medical diagnosis, non-invasive monitoring**

I. Introduction

NEURODEGENERATIVE diseases result from a progressive loss of structure or function of neurons, including the death of neurons. Alzheimer's disease is the most common form of neurodegenerative disease and is considered the sixth leading cause of death in the United States [1]-[2]. According to the Alzheimer's Association in U.S.A., Alzheimer's disease is the most expensive disease in the U. S., costing more than cancer and heart disease. In addition, the Alzheimer's Society in the UK reported that there are more than 520,000 people with Alzheimer's disease out of the 850,000 people suffering from dementia, with numbers expected to rise to 1 million by 2025. Symptoms include: substantial memory loss, problems with language, disorientation, loss in concentration, mood swings, behavioral issues, and eventually leading to loss of bodily functions and death [3]. The life expectancy of those diagnosed with Alzheimer's disease is between 3 to 9 years [3].

One of the distinguishing features of Alzheimer's disease is the progressive shrinkage of the brain due to atrophy (or the shrinkage of the brain) [4]. It has been found that the brain volume can reduce by more than 22% of the normal brain in Alzheimer's patients and that the brain's weight after Alzheimer's disease frequently falls under 1 kg as compared to the normal adult brain weight of 1.2 to 1.4 kgs [5]. Another distinguishing pathological change that occurs as a result of Alzheimer's disease is that the lateral ventricle enlarges as the disease progresses.

Detection and imaging of neurodegenerative diseases, such as Alzheimer's disease, has been the focus of research studies in the past decade. In previous studies, computed tomography (CT) and magnetic resonance imaging (MRI) were used to diagnostically rule out other causes of dementia [6]. Structural MRI is a recently developed tool that can be used to assess atrophy and changes in tissue characteristics [6]. An advantage of MRI is its availability and has been recommended extensively in the diagnosis of dementia in European and U.S. practices [6]. However, this comes at a high cost, which makes it difficult for some patients to pay for, and may not be readily available in certain countries. In addition, patients with a severe case of Alzheimer's disease may not tolerate MRI procedures, or CT scans.

In recent years, applications have been developed that utilized microwave technology to detect and image diseases in the brain such as stroke and brain tumor. An initial approach was discussed about in [7] where a Vivaldi antenna operating at a frequency range of 3 GHz to 10 GHz was simulated. The study reported it was able to detect a difference in scattered signals from a healthy head phantom and a head phantom that contained a tumor. However, due to the high frequency range the penetration was not strong enough to detect any anomalies beyond the region near the skull. Another Vivaldi antenna was proposed in [8] that operates between 1 GHz to 4 GHz. This antenna was able detect the occurrence of stroke in the head region. However, the study utilized a switching system using microwave coaxial switches in order to connect the elements of the array. As a result, the system was large and

This paper was submitted on May 29, 2019.
I. M. Saied and T. Arslan are with the University of Edinburgh, Edinburgh, UK EH9 3JW (Email: Imran.Saied@ed.ac.uk, Tughrul.Arslan@ed.ac.uk)

therefore, could only be used for static testing. A small portable UWB antenna system was discussed about in [9] and [10]. The portable system contained a portable vector network analyzer (VNA) that was custom-made for this setup. Its purpose was to replace the more conventional and bulkier VNA that would have limited the portability of this device. A textile-based antenna was discussed in [6] for proposed use in microwave head imaging. This antenna operated in the range of 1.2 GHz to 6 GHz. Although the antenna provided good SAR values and S_{11} results which are in line with the specifications need for a safe head imaging system, the size of the antenna was too big to create a proper array. In [11] and [12], a novel wearable antenna array system was designed for head imaging. The wearable head imaging system utilizes 8 flexible directional UWB monopole antennas. To ensure flexibility, the antennas were created using a very thin flexible polyethylene terephthalate (PET) substrate with a thickness of 75 um. The antennas operated at a frequency range between 1.3 GHz to 3.5 GHz that would allow sufficient penetration and resolution. The flexible nature of the antenna and implementation in clothing fabrics makes the device wearable and portable to the user. The device was simulated and tested using a VNA and was found to have satisfactory results for S_{11}. In addition, SAR value was found to be well below the maximum limit, thus making it a safe device to use on the human body. However, the device is fairly novel and more studies need to be performed in order to see how well the system works.

This paper presents a novel application of a low-cost and non-invasive wearable device to monitor the progression of brain atrophy and lateral ventricle enlargement in patients with Alzheimer's disease. Simulation and experimental results of the antennas in the device were used to detect the progression of brain atrophy using real lamb brains that were placed in a model of a human skull. The antennas used were a monopole, bi-directional antenna, created using a very thin flexible polyethylene terephthalate (PET). A vector network analyzer (VNA) was used to generate the signals to the antennas and also receive them for analysis. The reflection coefficients (S_{11}) and transmission coefficients (S_{21}) of the antennas were captured and analyzed in order to determine whether a correlation exist between the brain atrophy and lateral ventricle enlargement rates and captured measurements. To the best of the authors' knowledge, no prior research study has been made using this technology.

II. Antenna Design

The antennas were designed in order to be conformable and directional. In order to utilise a radar-based approach for microwave imaging, the designed antennas should exhibit ultra-wideband (UWB) performance. For this application, a planar monopole antenna is one of the best candidates due to its low-profile configuration as compared to a Vivaldi antenna, which has a high-profile structure along the direction of propagation, thus making it unsuitable for wearable applications. At low frequency levels, the antennas can achieve more penetration but less resolution. At high frequencies, on the other hand, the antennas can achieve less penetration but higher resolution. By using UWB antennas, the aim is to achieve good penetration and resolution for the antennas, so that they can be utilized eventually for radar-based imaging. Fig. 1 (a) shows a screenshot of the fabricated UWB antenna that was designed and used in this study, and 1 (b) shows the design of the UWB antennas. The values of the antenna's dimensions as shown in the schematic diagram are the following (in mm): $L = 70$, $W = 30$, $g = 0.5$, $L_f = 20$, $W_f = 7$, and $L_{tri} = 44$.

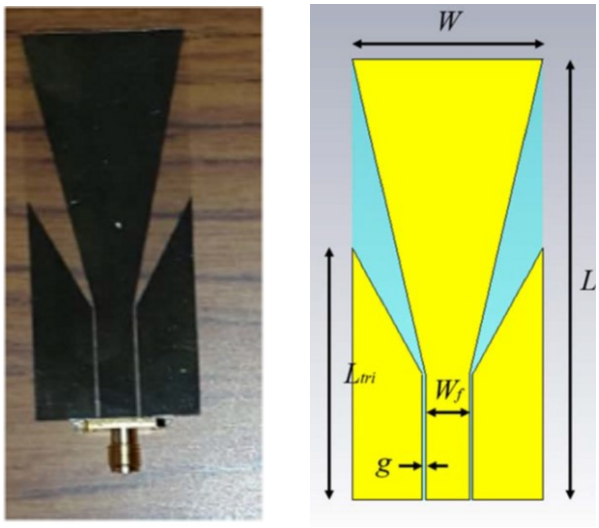

(a) (b)

Fig. 1. (a) Screenshot of fabricated UWB antenna. (b) Schematic diagram of the designed antenna.

The feeding line is made of a co-planar waveguide (CPW) structure where its characteristic impedance is 50 ohms, while a trapezoidal patch was selected as the radiating element in order to provide a smooth transition of the input current from the feeding line to the radiating elements, ensuring good impedance matching across the intended frequency. The substrate used for the antenna is PET that has a dielectric constant of 2.4 and a thickness of 75 µm, which provides flexibility to the antenna structure. The metallization is only on one side of the antenna structure.

III. Methods and Procedures

A. Simulation Methods

The simulations for testing the antenna measurements for brain atrophy and lateral ventricle enlargement were performed in near field using CST Microwave Suite. In order to simulate the brain atrophy tests, a realistic human head model was used that contained several tissues, such as: skin, skull, blood, white matter, and gray matter. A pair of monopole antennas were designed in CST and defined to be have material properties associated with PET material. The dielectric constant of the substrate used is 2.4. To ensure good penetration into the head, a working frequency between 0.8 and 3 GHz was utilized in the design of this

antenna. These antennas were placed on each side of the human head model next to the skin and near field measurements were obtained in the simulations. Characteristics of brain atrophy were simulated by uniformly reducing the size of the inner objects (i.e., white matter and gray matter), replacing the gap with cerebrospinal fluid, and keeping the size of the other objects (i.e. skull, skin, and blood) constant. After specifying the size of the brain, the simulation would be performed to capture S_{11} and S_{21} data from the antennas based on the different sizes of the brain in simulation. Fig. 2 shows the screenshot of the simulation model used in CST

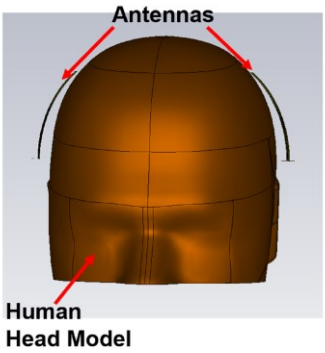

Fig. 2. Human head CST model and antennas that were used for simulations of brain atrophy and lateral ventricle enlargement.

In order to simulate lateral ventricle enlargement in CST, the same human head model was used with the same properties. However, an additional object was placed inside the gray matter layer and was defined to have properties of cerebral spinal fluid (CSF). This last layer was first defined to have a very small volume within the brain. As in the previous simulation for brain atrophy, the two PET antennas were designed and placed on the sides of the outer layer. To show the lateral ventricle size expanding, the size of the object corresponding to cerebral spinal fluid would be enlarged to different sizes. S_{11} and S_{21} data would then be measured and compared for different sizes of lateral ventricles within the brain.

B. Experimental Methods

The wearable device was constructed in a hat-like shape. The advantage of this structure is that it can be conveniently worn by patients. 6 monopole antennas are then arranged around the inner side of the absorber using Velcro, and the distance between each antenna is approximately 17 mm. The antennas are separated from the absorber using 5 mm thick foam whose dielectric constant is similar to that of air in order to maintain the antennas' integrity and not have its signals affected. The top of the device is made hollow in order to accommodate wires going from the antennas to the vector network analyzer (VNA), which controls the signals being generated and received by the antennas.

The system setup that was used for experiments is shown in Fig. 3. The experimental setup consists of a PC, VNA, wearable RF device, and the skull model which contains the fabricated phantoms. The experiments were conducted using a host PC that was connected to the VNA via a GPIB. The PC allows the user to setup the VNA and send a command to the VNA to start generating signals and capturing S_{11} and S_{21} data from the ports directly into the PC using a built-in software. The VNA that was used for the experiments is a HP 8753 that has a frequency range of 300 kHz to 3 GHz with a dynamic range of up to 100 dB. The wearable device was connected to 50-ohm ports on the VNA using SMA cables. Calibration was performed by first attaching the antennas inside the wearable device. Then the VNA was calibrated using the open, short, and load connections for each antenna. The device would then be placed on top of the skull model with no phantom inside. The S_{11} measurement would then be recorded and utilized as the benchmark for all other measurements.

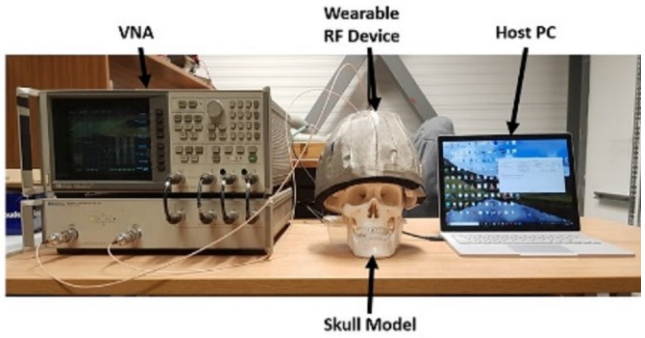

Fig. 3. Experimental setup consisting of Host PC, VNA, and Skull Model with wearable RF device.

For the experiments, a life-size skull model was used containing similar indentations that are present in human beings. In addition, the skull model could be disassembled easily, allowing contents to be placed inside. To create a realistic representation of a human brain, real lamb brains were used and placed inside the skull model. A typical lamb brain is about $1/10^{th}$ the size of a human brain. As a result, 10 whole lamb brains were molded into the skull cavity and frozen in order to provide the representation of a complete normal brain structure with a volume of 1200 cm^3.

To mimic the characteristics of brain atrophy in this first experiment, a measured amount of the lamb brain sample was removed uniformly around the outer layer for each atrophy case and replaced with a layer of artificial phantom that represents cerebrospinal fluid (CSF). This phantom was fabricated using salty water, agar, and a color dye to make it distinguishable in the experiments. For example, in the first experiment, 5% of the lamb brain was removed uniformly around the outer layer of the lamb brain. This empty region is replaced with an artificial phantom to mimic the characteristics of CSF. In the second experiment, another 5% of the lamb brain was removed again and replaced with a thicker layer of the artificial CSF phantom, resulting in a total decrease of 10% from the original complete model. Finally, for the third and fourth experiments, a 20% reduced-sized lamb brain model and a 25% reduced-sized lamb brain model were used respectively. Figs. 4(a)-(e) show images of the actual lamb brain skull models used in the brain atrophy experiments.

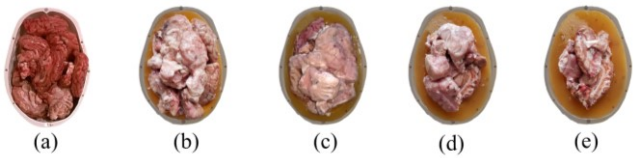

Fig. 4. Images showing different compositions of lamb brains and outer CSF layer (light brown color) inside the skull model representing brain atrophy for the following cases: a) full brain volume, b) 5%, c) 10%, d) 20%, and e) 25% brain atrophy, respectively.

To perform the second part of the experiments for detecting lateral ventricle enlargement, objects were created to mimic the CSF inside the brain. The same full-brain lamb brain sample was used and placed in the skull model; however, a 6-mm diameter cavity was created in both halves of the brain in order to insert the CSF object inside the brain. This 6-mm diameter cavity was created by first filling both halves of the skull model with lamb brains and then placing a plastic ball in the center of these halves. The model would then be frozen to ensure that the lamb brains remain fixed in the same location. Once frozen, the plastic ball would be removed and the resulting cavity is created. Fig. 5 (a) shows the resulting cavity that was created in one half of the skull model.

To create the CSF objects, different sizes of an artificial phantom were created using water, salt, and agar in order to create a high dielectric object and inserted into the cavity (shown in Figs. 5 (b)-(e)). Once inserted into the cavity, the lamb brains would be allowed to thaw out so that it can conform around the shape of the CSF object and fill up any gaps left behind. A green color dye was utilized to make the objects distinguishable in the experiments. The volumes of the samples were: 1) 22.6 mm^3, 2) 56.5 mm^3, 3) 113 mm^3, and 4) 226 mm^3.

Fig. 5. Images of: (a) frozen lamb brain with 6-mm diameter cavity and (b)-(e) different-sized CSF samples (light green color) used in the experiments: b) 22.6 mm^3, c) 56.5 mm^3, d) 113 mm^3, and e) 226 mm^3.

IV. Results

A. Simulation Results

Fig. 6 shows changes in S_{11} plots for different brain atrophy cases compared to the S_{11} plot of a normal full-size brain with a *mean* ± *standard deviation* of −7.4400 ± 5.8268. It can be noticed that as the brain volume decreases, there is an overall downward shift in the S_{11} graph indicating more loss in the signal as they do not get reflected back. 5% brain atrophy shows an insignificant change in the S_{11} plots due to the small amount of change in the brain size. However, for the case of 20% and 25% brain atrophy, at 1.5 GHz, the signal loss is almost double the S_{11} value associated with the full brain case, thus validating the antennas' capability of detecting brain atrophy in reflection mode.

Fig. 7 shows changes in S_{21} plots for different brain atrophy cases based on simulations compared to the S_{21} of a normal brain with a *mean* ± *standard deviation* of −57.3593 ± 7.4864. The plots indicate that as the brain's size decreases, a downward shift in the S_{21} plots is present, indicating that the signal is not transmitted properly to the other antenna due to the decrease in brain tissues and increase in the higher-dielectric CSF layer that absorbs most of the transmitted signals.

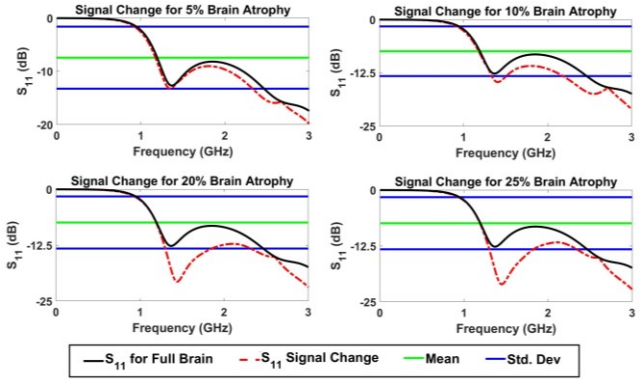

Fig. 6. Simulation plots showing changes in reflection coefficient (S_{11}) between a normal brain and brain with 5%, 10%, 20%, and 25% brain atrophy.

This trend can be seen in the case of 20% and 25% brain atrophy where the change in S_{21} is between 20 and 40 dB across the bandwidth between 0.84 GHz to 2.4 GHz, which corresponds with the antennas' operating frequency range. This proves that based on simulations, the antennas are able to detect brain atrophy in transmission mode.

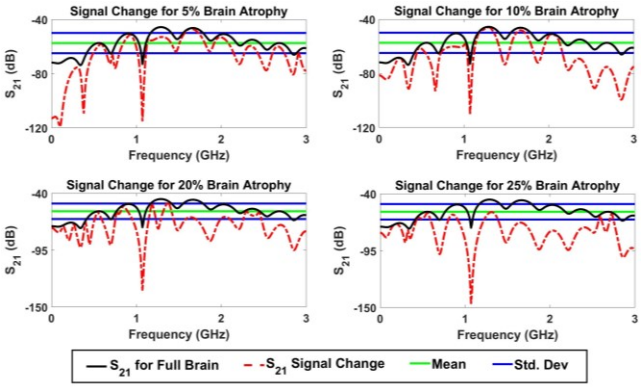

Fig. 7. Simulation plots showing changes in transmission coefficient (S_{21}) between a normal brain and brain with 5%, 10%, 20%, and 25% brain atrophy.

Simulations for lateral ventricle enlargement were also conducted and results were analyzed. Fig. 8 shows changes in S_{11} plots obtained from simulations between a brain with no CSF in the brain, with a *mean* ± *standard deviation* of

−7.3700 ± 5.6154, and one with CSF levels increased by 2 times and 4 times in the lateral ventricles, respectively.

As the amount of cerebral spinal fluid increases in the brain from 2 times to 4 times the amount, the S_{11} plots shows an increasing downward shift in the reflected signal, which indicates an increased loss in the signal. This is due to the higher dielectric difference of the CSF object compared to brain tissues. The change in the S_{11} loss increases from −11 dB to −17.5 dB at 1.35 GHz when a quadruple increase in CSF object occurs in the lateral ventricle. This validates the antennas' ability to detect lateral ventricle enlargement in the reflection mode.

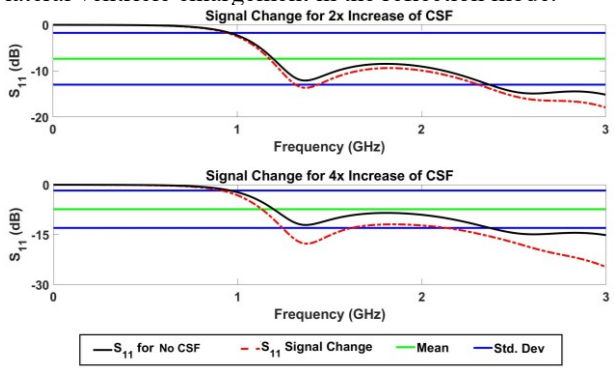

Fig. 8. Simulation plots showing changes in S_{11} between a brain with normal CSF levels and brain with 2x and 4x CSF levels in the lateral ventricles.

Simulations were also performed to investigate the transmission characteristics due to increasing lateral ventricle sizes and shown in Fig. 9.

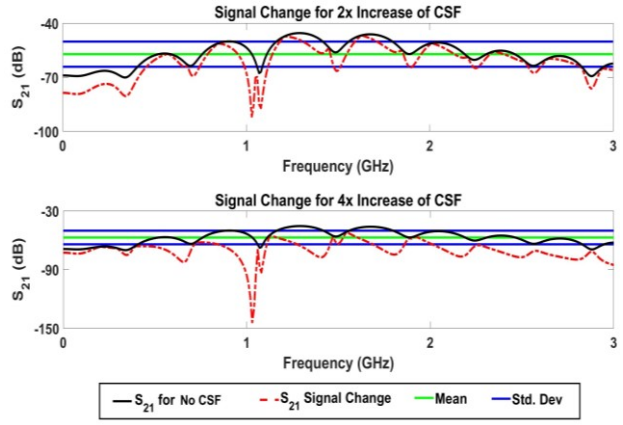

Fig. 9. Simulation plots showing changes in S_{21} between a brain with normal CSF levels and brain with 2x and 4x CSF levels in the lateral ventricles.

In Fig. 9, the plot for a brain with no CSF in the ventricle has a *mean* ± *standard deviation* of −57.2078 ± 6.9762. As the levels of CSF increases, a downward shift is present in the S_{21} plots that is significant between 0.84 GHz and 1.5 GHz. This loss is due to the CSF in between that hinders the signal from transmitting to the other antenna. In addition, when the size of the CSF increases from 2 times to 4 times, the S_{21} plot at 1.05 GHz shows a sudden increase in the loss from −86 dB to −150 dB. This result validates that the antennas are capable of detecting lateral ventricle enlargement in the transmission mode.

Table I summarises the statistical results of the simulation models for brain atrophy and increasing ventricle cases. The mean, standard deviation, p-value (*p*), and resulting null hypothesis (*h*) have been recorded for each of the cases. For this study, the significance level of *p* was chosen to be at 0.05 or 5%. In addition, $h = 0$ represents that the null hypothesis was not rejected, while $h = 1$ indicates the rejection of the null hypothesis, respectively.

TABLE I
STATISTICAL RESULTS OF SIMULATION MODELS

Simulation Cases	P-Value (S_{11})	*H* (S_{11})	P-Value (S_{21})	*H* (S_{21})
Brain Atrophy				
5% Brain Atrophy	0.0496	1	0.0367	1
10% Brain Atrophy	0.0378	1	5.97E-10	1
20% Brain Atrophy	0.0037	1	2.78E-12	1
25% Brain Atrophy	0.0049	1	7.36E-24	1
Lateral Ventricle Enlargement				
2x Increase of CSF	0.0401	1	0.0286	1
3x Increase of CSF	0.0225	1	3.41E-8	1

Based on the statistical data provided in Table I, it can be seen that for all cases, *p* is less than 0.05, and therefore the null hypothesis can be rejected, thus concluding that the antennas are capable of detecting changes in brain atrophy and lateral ventricle sizes in the operating frequency range.

B. Experimental Results

Results were obtained from experiments and compared with those from simulations to verify antennas' capability of detecting brain atrophy and lateral ventricle enlargement. Figs. 10 and 11 show the plots of changes in S_{11} and S_{21} respectively between different cases of brain atrophy and a normal full brain. The S_{11} plot of a normal full brain has a *mean* ± *standard deviation* of −9.1587 ± 6.1556, while the S_{21} plot has a *mean* ± *standard deviation* of −25.1777 ± 7.0757, respectively.

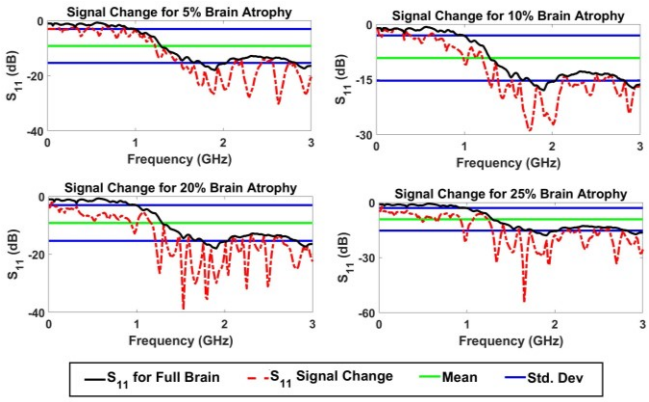

Fig. 10. Plots showing changes in reflection coefficient (S_{11}) between a normal brain and brain with 5%, 10%, 20%, and 25% brain atrophy obtained from experiments.

Fig. 10 shows that as brain atrophy increases, the resulting S_{11} plots displays more loss in the signal and therefore an oscillating downward shift in the overall trend between 0.8 to 2.5 GHz. Oscillations may be due to noise that is emitted from the surroundings in the experimental setup. However, the overall trend is expected based on simulation results and verifies the antennas' ability to detect brain atrophy in the reflection mode. In particular, the change in S_{11} loss increases significantly to −30 dB, −40 dB, and −55 dB for 10%, 20%, and 25% brain atrophy cases, respectively.

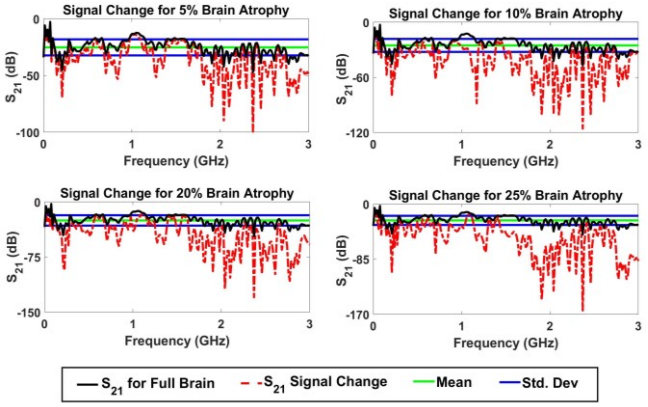

Fig. 11. Plots showing changes in S_{21} between a normal brain and brain with 5%, 10%, 20%, and 25% brain atrophy obtained from experiments.

Similarly, S_{21} plots in Fig. 11 show that as brain atrophy increases, there is more loss displayed in the transmitted signal due to the increasing presence of a thicker CSF layer that hinders the signal from transmitting to the receiving antenna. This leads to a larger difference in S_{21} data that can be seen in 10%, 20%, and 25% brain atrophy cases, respectively. In addition, both the S_{11} and S_{21} plots show this behavior occurring in the frequency range of 0.85 GHz to 2.6 GHz which corresponds with the operating frequency of the antenna design.

Experiments were also performed for lateral ventricle enlargement and its resulting S_{11} and S_{21} plots are shown Figs. 12 and 13 respectively. The S_{11} plot for no CSF has a *mean* ± *standard deviation* of −10.0821 ± 5.9123, while the S_{21} plot has a *mean* ± *standard deviation* of −25.6884 ± 4.7394, respectively.

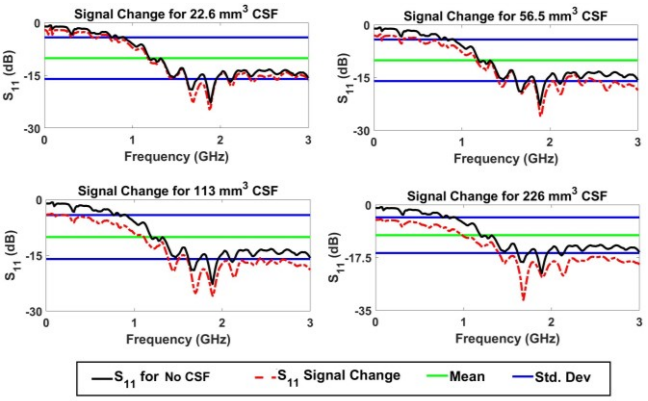

Fig. 12. Plots showing changes in S_{11} signals obtained from experiments for increasing volumes of CSF as a result of lateral ventricle enlargement.

Results in Fig. 12 shows a similar trend found in the simulation results where the S_{11} loss increases as a result of increasing CSF volume, due to the change in the dielectric properties. This pattern is also present in the S_{21} plots in Fig. 13 as well where the transmitted signal is not propagated completely to the receiving antenna due to the increasing CSF sample that hinders the signal in between. This characteristic can be seen between 0.86 to 1.7 GHz, where the change in S_{21} is increased to almost three times the original value. Therefore, the antennas are capable of detecting lateral ventricle enlargement in both reflection and transmission modes.

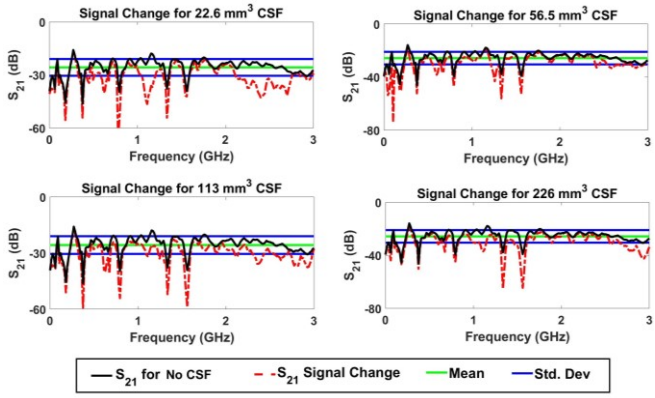

Fig. 13. Changes in S_{21} plots obtained from experiments for increasing volumes of CSF as a result of lateral ventricle enlargement.

Table II summarises the statistical results of the experiments for brain atrophy and increasing ventricle cases. As in Table I, p-value (p) and resulting null hypothesis (h) have been recorded for each of the cases, while significance level of p was chosen to be at 0.05 or 5%. It can be seen that for all the experiments, p is less than 0.05, and therefore the null hypothesis is rejected. As a result, this concludes that the antennas are genuine in detecting changes in brain atrophy and lateral ventricle sizes in practical applications as well.

TABLE II
STATISTICAL RESULTS OF EXPERIMENTS

Experiments	P-Value (S_{11})	H (S_{11})	P-Value (S_{21})	H (S_{21})
Brain Atrophy				
5% Brain Atrophy	0.0498	1	1.47E-11	1
10% Brain Atrophy	0.0484	1	6.67E-4	1
20% Brain Atrophy	0.0249	1	3.84E-14	1
25% Brain Atrophy	0.0038	1	4.82E-17	1
Lateral Ventricle Enlargement				
22.6 mm^3 CSF	0.0442	1	0.0389	1
56.5 mm^3 CSF	0.012	1	0.0288	1
113 mm^3 CSF	5.8E-7	1	0.0248	1
226 mm^3 CSF	1.41E-11	1	0.0014	1

A closed form expression can also be proposed that provides a general relationship between the S-parameters and the amount of either brain atrophy or lateral ventricle enlargement that occurs in the brain. To obtain such expressions, curve fitting analysis was performed in MATLAB on the measured data for the cases of brain atrophy and lateral ventricle enlargement, separately. Using the curve fitting toolbox in MATLAB, a general expression was obtained for percentage change in S_{11} and S_{21} parameters with respect to the level of brain atrophy and lateral ventricle enlargement separately.

In order to verify that the obtained equations fit the model, the following conditions were evaluated as part of the goodness of fit criteria for this study:

1. Sum of squares due to error (SSE) should be close to 0.
2. R-square should be greater than 0.85 and less than 1.
3. Adjusted R-square should be greater than 0.85 and less than 1.
4. Root mean squared error (RMSE) should be close to 0.

Based on these conditions, the following closed form expressions were obtained for percentage change in S_{11} (1) and S_{21} (2) with respect to level of change in brain atrophy:

$$\begin{aligned} \%\ change\ in\ S_{11} = {} & -1.41 + 0.068\cos(1.05x) \\ & + 2.21\sin(1.05x) + 1.29\cos(2.1x) \\ & - 0.077\sin(2.1x) - 0.028\cos(3.15x) \\ & - 0.46\sin(3.15x) \end{aligned} \quad (1)$$

$$\begin{aligned} \%\ change\ in\ S_{21} = {} & -55.83 - 11.19\cos(1.63x) \\ & - 0.44\sin(1.05x) - 2.32\cos(3.26x) \\ & - 0.79\sin(3.26x) + 2.03\cos(4.89x) \\ & + 2.297\sin(4.89x) \end{aligned} \quad (2)$$

where x is the percentage of brain atrophy. In addition, the curve fitting approach was utilized to obtain closed form equations for percentage change in S_{11} (3) and S_{21} (4) respectively based on the level of lateral ventricle enlargement in the brain.

$$\begin{aligned} \%\ change\ in\ S_{11} = {} & -0.04 + 0.037\cos(1.11y) \\ & - 0.02\sin(1.11y) - 0.02\cos(2.22y) \\ & - 0.05\sin(2.22y) - 0.025\cos(3.32y) \\ & + 0.02\sin(3.32y) \end{aligned} \quad (3)$$

$$\begin{aligned} \%\ change\ in\ S_{21} = {} & -0.065 - 0.012\cos(5.74y) \\ & + 0.01\sin(5.74y) - 0.007\cos(11.48x) \\ & + 0.012\sin(11.48y) + 0.01\cos(17.2y) \\ & + 0.035\sin(17.2y) \end{aligned} \quad (4)$$

where y is the volume of CSF inside the lateral ventricles.

Finally, the specific absorption rate (SAR) was also calculated through simulations in CST to investigate the effects of the EM wave exposure from the device to the human head. The maximum limit of SAR approved by the UK government is 2W/kg for 10g of tissue mass, which must be complied to ensure safe operation of the wearable device. At 1.5 GHz, the SAR values were found to be 0.0115 W/kg, 0.115 W/kg, and 1.15 W/kg for transmitted power of 1 mW. 10mW, and 100 mW respectively. At 2.5 GHz, the SAR values were found to be 0.0121 W/kg, 0.122 W/kg, and 1.2112 W/kg for 1 mW, 10 mW, and 100 mW respectively. Finally, at 3 GHz, the calculated SAR values were 0.135 W/kg, 0.133 W/kg, and 1.355 W/kg for 1 mW, 10mW, and 100 mW respectively. It can be seen that for each frequency, the calculated SAR values are well below the maximum limit indicated by the UK government. In addition, the EM waves absorbed by the biological tissue increases linearly with the transmitted power. Based on these results, it is therefore recommended to limit the transmitted power to below 100 mW to ensure safe operation of the wearable device.

V. Conclusions

Simulations and experiments were performed to verify the design of a novel device capable of monitoring the progression of brain atrophy and lateral ventricle enlargement in the brain as a result of Alzheimer's disease. The device contained UWB antennas that operated between 0.8 and 3 GHz. The non-invasive monitoring approach and wearable design makes it a novel tool for medical diagnostic devices. Results from simulations and experiments show that the antennas in the device are capable of detecting different levels of brain atrophy and lateral ventricle enlargement in both the reflection and transmission modes, thus providing a promising tool for monitoring patients with Alzheimer's disease. This study is the foundation for future work to be performed in developing early-stage Alzheimer's disease detection approaches. Future work will focus on investigating techniques that adapt and test the device on different head sizes. This would lead to a revolutionary non-invasive technology that would solve a major challenge of Alzheimer's disease and provide a way for early diagnosis.

References

[1] C. A. Taylor, S. F. Greenlund, L. C. McGuire, H. Lu, J. B. Croft, "Deaths from Alzheimer's Disease-United States, 1999-2014," *MMWR Morb Mortal Wkly Report*, vol. 66, pp. 521-526, 2017.

[2] Alzheimer's Association, "2017 Alzheimer's disease facts and figures," *Alzheimer's Dementia Journal*, vol. 4, pp. 459-509, 2017.

[3] H. W. Querfurth, F. M. LaFerla, "Alzheimer's disease," *The New England Journal of Medicine*, vol. 362, no. 4, pp. 329–344, 2010.

[4] C. A. Raji et al. "Age, Alzheimer Disease, and Brain Structure," Neurology, vol. 73.22, pp. 1899–1905, 2009.

[5] R. Peters, "Ageing and the Brain." *Postgraduate Medical Journal*, vol. 82.964, pp. 84–88, 2006.

[6] K. A. Johnson, N. C. Fox, R. A. Sperling, and W. E. Klunk, "Brain imaging in Alzheimer disease," *Cold Spring Harb Perspect Med.*, vol. 4, pp. 1-23, 2012.

[7] Z. Haoyu, A. O. El-Rayis, N. Haridas, N. H. Noordin, A. T. Erdogan, and T. Arslan, "A smart antenna array for brain cancer detection," in *Antennas and Propagation Conference (LAPC), 2011 Loughborough*, vol. no. pp. 1-4, 14-15 Nov. 2011.

[8] B. J. Mohammad, A. M. Abbosh, S. Mustafa, and D. Ireland, "Microwave System for Head Imaging," *IEEE Transactions on Instrumentation and Measurement*, vol. 63, no. 1, pp. 117-123, Jan 2014.

[9] A. T. Mobashher, A. M. Abbosh, and Y. Wang, "Microwave System to Detect Traumatic Brain Injuries Using Compact Unidirectional Antenna and Wideband Transceiver with Verification on Realistic

Head Phantom," *IEEE Transactions on Microwave Theory and Techniques*, vol. 62, no. 9, pp. 1826-1836, Sept 2014.

[10] S. A. Rezaeieh, A. Zamani, and A. M. Abbosh, "3-D Wideband Antenna for Head-Imaging System with Performance Verification in Brain Tumor Detection," *IEEE Antennas and Wideband Propagation Letters*, vol. 14, no., pp. 910-914, 2015.

[11] M. S. R. Bashri, T. Arslan, W. Zhou, and N. Haridas, "Wearable Device for Microwave head Imaging," *46th European Microwave Conference*, pp. 671-674, 2016.

[12] M. S. R. Bashri, T. Arslan, and W. Zhou, "Flexible Antenna Array for Wearable Head Imaging System," 2017 11th European Conference on Antennas and Propagation (EUCAP), pp. 172-176, 2017.

Imran M. Saied obtained his B.Sc. in Electrical Engineering from Georgia Institute of Technology in 2009 and his M.Sc. in Electrical Engineering from California State University-Fullerton in 2011. He is currently pursuing his PhD at the University of Edinburgh, where he focuses his research on investigating the use of RF and microwaves for detecting neurodegenerative diseases.

He has an extensive global work experience spanning across U.S.A., India, and U.A.E. Prior to beginning his PhD, he worked as a Research Assistant for the Petroleum Institute (now Khalifa University) in Abu Dhabi, U. A. E. from 2013 to 2017. He worked on developing several tomography and spectroscopy systems for real-time oil and gas pipeline monitoring systems. In particular, he focused on THz spectroscopy, ECT/ECAT tomography, and development of sensors and imaging algorithms for these systems. The results that have been obtained from his work have led to several refereed journal and conference papers that have been published in IEEE and SPE.

Prof. T. Arslan holds the Chair of Integrated Electronic Systems in the School of Engineering, University of Edinburgh, Edinburgh, UK. He is a member of the Integrated Micro and Nano Systems (IMNS) Institute and leads the Embedded Mobile and Wireless Sensor Systems (Ewireless) Group in the University (ewireless.eng.ed.ac.uk). His current research focuses on developing low power radio frequency sensors for wearable and portable biomedical applications. He is the author of over 500 refereed papers and inventor of over 20 patents.

Prof. Arslan is currently an Associate Editor of IEEE Transactions on VLSI Systems and was previously an Associate Editor for the IEEE Transactions on Circuits and Systems I (2005-2006), IEEE Transactions on Circuits and Systems II (2008-2009). He is also a member of the IEEE CAS executive committee on VLSI Systems and Applications (1999 to date), and is a member of the steering and technical committees of a number of international conferences. He is a co-founder of the NASA/ESA conference on Adaptive Hardware and Systems (AHS) and currently serves as a member of its steering committee.